Computers and Concrete, *Vol. 20, No. 3 (2017) 361-368*
DOI: https://doi.org/10.12989/cac.2017.20.3.361

Seismic response of concrete columns with nanofiber reinforced polymer layer

Mohsen Motezaker[1] and Reza Kolahchi*[2]

[1]*Department of Civil Engineering, School of Science and Engineering, Sharif University of Technology, International Campus, Kish Island, Iran*
[2]*Department of Civil Engineering, Meymeh Branch, Islamic Azad University, Meymeh, Iran*

(Received May 26, 2017, Revised June 28, 2017, Accepted June 29, 2017)

Abstract. Seismic response of the concrete column covered by nanofiber reinforced polymer (NFRP) layer is investigated. The concrete column is studied in this paper. The column is modeled using sinusoidal shear deformation beam theory (SSDT). Mori-Tanaka model is used for obtaining the effective material properties of the NFRP layer considering agglomeration effects. Using the nonlinear strain-displacement relations, stress-strain relations and Hamilton's principle, the motion equations are derived. Harmonic differential quadrature method (HDQM) along with Newmark method is utilized to obtain the dynamic response of the structure. The effects of different parameters such as NFRP layer, geometrical parameters of column, volume fraction and agglomeration of nanofibers and boundary conditions on the dynamic response of the structure are shown. The results indicated that applied NFRP layer decreases the maximum dynamic displacement of the structure. In addition, using nanofibersas reinforcement leads a reduction in the maximum dynamic displacement of the structure.

Keywords: seismic response; NFRP layer; SSDT; HDQM; newmark method

1. Introduction

The study of the application of nanotechnology in the construction industry and building structures is one of the most prominent priorities of the research community. The outstanding chemical and physical properties of nanomaterials enable several applications ranging from structural reinforcement to environmental pollution remediation and production of self-cleaning materials. It is known that concrete is the leading material in structural applications, where stiffness, strength and cost play a key role in the high attributes of concrete.

With respect to the analysis of concrete structures, to investigate the seismic behavior of connections composed of steel reinforced ultra high strength concrete (SRUHSC) column and reinforced concrete (RC) beam, six interior strong-column-weak-beam connection specimens were tested by Yan *et al.* (2010) subjected to reversal cyclic load. the seismic behavior of short circular reinforced concrete columns was studied by Zong-Cai *et al.* (2014) testing seven columns retrofitted with prestressing steel wire (PSW), subjected to combined constant axial compression and lateral cyclic load. Nominal moment-axial load interaction diagrams, moment-curvature relationships, and ductility of rectangular hybrid beam-column concrete sections were analyzed by El-Helou and Aboutaha (2015) using the modified Hognestad concrete model. A novel optimization approach for reinforced concrete (RC) biaxially loaded columns is proposed. Since there are several design constraints and influences, a new computation methodology using iterative analyses for several stages was proposed by Nigdeli *et al.* (2015). A new structural damage index for seismic fragility analysis of reinforced concrete columns was developed by Kang and Lee (2016) based on a local tensile damage variable of the Lee and Fenves plastic-damage model. Finite element (FE) method based Numerical investigation for evaluation of axial strength of SSWM strengthened plain cement concrete (PCC) and reinforced cement concrete (RCC) columns was presented by Kumar and Patel (2016). Simplified P-M interaction curve model for reinforced concrete columns exposed to standard fire was studied by Lee *et al.* (2017). The nonlinear buckling of straight concrete columns armed with single-walled carbon nanotubes (SWCNTs) and SiO2 nanoparticles resting on foundation was investigated by Jafarian Arani *et al.* (2016) and Zamanian *et al.* (2016). The nonlinear buckling of straight concrete columns armed with single-walled carbon nanotubes (SWCNTs) resting on foundation was investigated by Safari Bilouei *et al.* (2016). Stress analysis of concrete pipes reinforced with AL_2O_3 nanoparticles was presented by Heidarzadeh *et al.* (2016) considering agglomeration effects. Buckling of horizontal concrete columns reinforced with Zinc Oxide (ZnO) nanoparticles was analyzed by Arbabi *et al.* (2017).

For the first time, dynamic response of NFRP strengthened concrete columns subjected to seismic excitation is studied in the present research. The concrete column is modeled by applying SSDT and the effective material properties of the NFRP layer are obtained based on Mori-Tanaka model. The dynamic displacement of structure

*Corresponding author, Professor
E-mail: r.kolahchi@gmail.com

ISSN: 1598-8198 (Print), 1598-818X (Online)

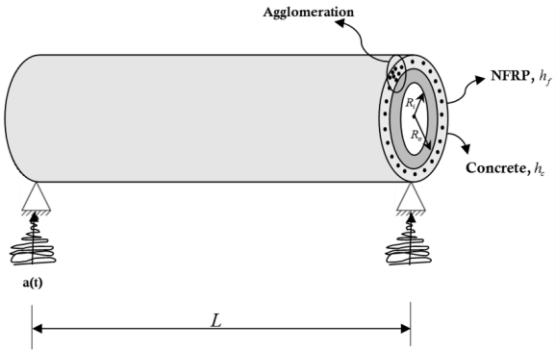

Fig. 1 A schematic figure for concrete columns with NFRP layer under seismic load

is calculated by HDQM in conjunction with Newmark method. The effects of different parameters such as NFRP layer, geometrical parameters of column, volume fraction and agglomeration of nanofibers and boundary conditions on the dynamic response of the structure are shown.

2. Formulation

In this section, the governing equations of the NFRP strengthened concrete columns are derived by applying SSDT to analyze the dynamic behavior of the structure. Fig. 1 illustrates a hollow circular concrete column subjected to the earthquake loads with outer radius of R_0, inner radius of R_i and thickness of h_c which strengthened by a NFRP layer with thickness of h_f.

By applying SSDT, the displacements fields are defined as below (Thai and Vo 2012)

$$\begin{aligned} u_1(x,z,t) &= u(x,t) - z\frac{\partial w(x,t)}{\partial x} + f\psi(x,t), \\ u_2(x,z,t) &= 0, \\ u_3(x,z,t) &= w(x,t), \end{aligned} \tag{1}$$

where u, v and w are the respective translation displacements of a point at the mid-plane of the beam in the longitudinal x, transverse y and thickness z directions. Also, ψ denotes the rotation of the cross section area and f is the shape function of the beam which is considered as follows

$$f = \frac{h}{\pi}\sin\left(\frac{\pi z}{h}\right). \tag{2}$$

in which $h=h_f+h_c$. However, the strain-displacement relations of the structure are given as below

$$\varepsilon_{xx} = \frac{\partial u}{\partial x} - z\frac{\partial^2 w}{\partial x^2} + \frac{1}{2}\left(\frac{\partial w}{\partial x}\right)^2 + f\frac{\partial \psi}{\partial x}, \tag{3}$$

$$\varepsilon_{xz} = \cos\left(\frac{\pi z}{h}\right)\psi. \tag{4}$$

The constitutive equations of the orthotropic beam are considered as below

$$\sigma_{xx}^c = C_{11}\varepsilon_{xx}, \tag{5}$$

$$\tau_{xz}^c = C_{44}\gamma_{xz}, \tag{6}$$

where C_{11} and C_{44} are the elastic constants of the concrete column. Also, the constitutive equations of the NFRP layer are defined as follows

$$\sigma_{xx}^f = Q_{11}\varepsilon_{xx}, \tag{7}$$

$$\tau_{xz}^f = Q_{44}\gamma_{xz}, \tag{8}$$

in which Q_{11} and Q_{44} are the elastic constants of the NFRP layer. To obtain the effective material properties of the NFRP layer and to consider the agglomeration effect, Mori-Tanak model is employed which is introduced in the next section.

3. Mori-Tanaka model

In this section, material properties of resin epoxy polymer reinforced by carbon nanofibers are obtained based on micro-mechanical approach. E_m and v_m are considered as Young's modulus and Poisson's ratio of the polymer, respectively. The stress-strain relations of the equivalent composite material are given as below (Mori and Tanaka 1973)

$$\begin{Bmatrix} \sigma_{11} \\ \sigma_{22} \\ \sigma_{33} \\ \sigma_{23} \\ \sigma_{13} \\ \sigma_{12} \end{Bmatrix} = \begin{bmatrix} k+m & l & k-m & 0 & 0 & 0 \\ l & n & l & 0 & 0 & 0 \\ k-m & l & k+m & 0 & 0 & 0 \\ 0 & 0 & 0 & p & 0 & 0 \\ 0 & 0 & 0 & 0 & m & 0 \\ 0 & 0 & 0 & 0 & 0 & p \end{bmatrix} \begin{Bmatrix} \varepsilon_{11} \\ \varepsilon_{22} \\ \varepsilon_{33} \\ \gamma_{23} \\ \gamma_{13} \\ \gamma_{12} \end{Bmatrix}, \tag{9}$$

where k, l, m, n and$p$ are known as Hill's elastic moduli so that, k is plane-strain bulk modulus normal to the fiber direction, n is the uniaxial tension modulus in the longitudinal direction of the fiber, l is the associated cross modulus, m and p are the shear moduli in planes normal and parallel to the fiber direction, respectively. It should be noted that the mentioned constants depends on the elastic constants of the material. For example, $Q_{11}=k+m$. By applying Mori-Tanaka model, Hill's elastic moduli can be obtained as follows (Mori and Tanaka 1973)

$$\begin{aligned} k &= \frac{E_m\{E_m c_m + 2k_r(1+\nu_m)[1+c_r(1-2\nu_m)]\}}{2(1+\nu_m)[E_m(1+c_r-2\nu_m)+2c_m k_r(1-\nu_m-2\nu_m^2)]}, \\ l &= \frac{E_m\{c_m\nu_m[E_m+2k_r(1+\nu_m)]+2c_r l_r(1-\nu_m^2)]\}}{(1+\nu_m)[E_m(1+c_r-2\nu_m)+2c_m k_r(1-\nu_m-2\nu_m^2)]}, \\ n &= \frac{E_m^2 c_m(1+c_r-c_m\nu_m)+2c_m c_r(k_r n_r - l_r^2)(1+\nu_m)^2(1-2\nu_m)}{(1+\nu_m)[E_m(1+c_r-2\nu_m)+2c_m k_r(1-\nu_m-2\nu_m^2)]} \\ &\quad + \frac{E_m[2c_m^2 k_r(1-\nu_m)+c_r n_r(1+c_r-2\nu_m)-4c_m l_r\nu_m]}{E_m(1+c_r-2\nu_m)+2c_m k_r(1-\nu_m-2\nu_m^2)}, \\ p &= \frac{E_m[E_m c_m + 2p_r(1+\nu_m)(1+c_r)]}{2(1+\nu_m)[E_m(1+c_r)+2c_m p_r(1+\nu_m)]}, \\ m &= \frac{E_m[E_m c_m + 2m_r(1+\nu_m)(3+c_r-4\nu_m)]}{2(1+\nu_m)\{E_m[c_m+4c_r(1-\nu_m)]+2c_m m_r(3-\nu_m-4\nu_m^2)\}}, \end{aligned} \tag{10}$$

in which k_r, l_r, n_r, p_r and m_r are Hill's elastic moduli of the reinforcing phase of the composite material. Finally by substituting Eq. (10) into Eq. (9), the stiffness matrix can be obtained. The experimental results show that the uniform distribution of the nanofibers is rarely achievable (Shu and Xue 1997). It is observed that the most of the nanofibers centralized in the regions throughout the matrix. These regions are assumed to be in spherical shapes which known as "inclusions" with different material properties from the surrounding regions. V_r is the total volume of nanofibersand is defined as

$$V_r = V_r^{inclusion} + V_r^m, \tag{11}$$

in which $V_r^{inclusion}$ and V_r^m represent the volume of the CNTs inside the inclusion and polymer matrix, respectively. The agglomeration effect can be considered based on the micro-mechanical model by introducing the two following parameters

$$\xi = \frac{V_{inclusion}}{V}, \tag{12}$$

$$\zeta = \frac{V_r^{inclusion}}{V_r}. \tag{13}$$

The average volume fraction C_r of nanofibers in the composite material is given as follows

$$C_r = \frac{V_r}{V}. \tag{14}$$

The volume fraction of nanofibers inside the inclusion and the matrix (concrete) can be defined as

$$\frac{V_r^{inclusion}}{V_{inclusion}} = \frac{C_r\zeta}{\xi}, \tag{15}$$

$$\frac{V_r^m}{V - V_{inclusion}} = \frac{C_r(1-\zeta)}{1-\xi}. \tag{16}$$

We assume that nanofibers are transversely isotropic and the orientation of them is randomly. Hence, the inclusion is considered to be isotropic and the effective bulk modulus K and shear modulus G may be written as below

$$K = K_{out}\left[1 + \frac{\xi\left(\frac{K_{in}}{K_{out}} - 1\right)}{1 + \alpha(1-\xi)\left(\frac{K_{in}}{K_{out}} - 1\right)}\right], \tag{17}$$

$$G = G_{out}\left[1 + \frac{\xi\left(\frac{G_{in}}{G_{out}} - 1\right)}{1 + \beta(1-\xi)\left(\frac{G_{in}}{G_{out}} - 1\right)}\right], \tag{18}$$

in which K_{in} and K_{out} are the effective bulk modulus of the inclusion and the matrix outside the inclusion, respectively. Also, G_{in} and G_{out} are the effective shear modulus of the inclusion and the matrix outside the inclusion, respectively and are given as follows

$$K_{in} = K_m + \frac{(\delta_r - 3K_m\chi_r)C_r\zeta}{3(\xi - C_r\zeta + C_r\zeta\chi_r)}, \tag{19}$$

$$K_{out} = K_m + \frac{C_r(\delta_r - 3K_m\chi_r)(1-\zeta)}{3[1-\xi - C_r(1-\zeta) + C_r\chi_r(1-\zeta)]}, \tag{20}$$

$$G_{in} = G_m + \frac{(\eta_r - 3G_m\beta_r)C_r\zeta}{2(\xi - C_r\zeta + C_r\zeta\beta_r)}, \tag{21}$$

$$G_{out} = G_m + \frac{C_r(\eta_r - 3G_m\beta_r)(1-\zeta)}{2[1-\xi - C_r(1-\zeta) + C_r\beta_r(1-\zeta)]}, \tag{22}$$

where χ_r, β_r, δ_r and η_r can be obtained as

$$\chi_r = \frac{3(K_m + G_m) + k_r - l_r}{3(k_r + G_m)}, \tag{23}$$

$$\beta_r = \frac{1}{5}\left\{\begin{array}{l}\frac{4G_m + 2k_r + l_r}{3(k_r + G_m)} + \frac{4G_m}{(p_r + G_m)} \\ + \frac{2[G_m(3K_m + G_m) + G_m(3K_m + 7G_m)]}{G_m(3K_m + G_m) + m_r(3K_m + 7G_m)}\end{array}\right\}, \tag{24}$$

$$\delta_r = \frac{1}{3}\left[n_r + 2l_r + \frac{(2k_r - l_r)(3K_m + 2G_m - l_r)}{k_r + G_m}\right], \tag{25}$$

$$\eta_r = \frac{1}{5}\left[\begin{array}{l}\frac{2}{3}(n_r - l_r) + \frac{4G_m p_r}{(p_r + G_m)} + \frac{2(k_r - l_r)(2G_m + l_r)}{3(k_r + G_m)} \\ + \frac{8G_m m_r(3K_m + 4G_m)}{3K_m(m_r + G_m) + G_m(7m_r + G_m)}\end{array}\right], \tag{26}$$

K_m and G_m are the bulk and shear moduli of the matrix phase which are defined as below

$$K_m = \frac{E_m}{3(1-2\upsilon_m)}, \tag{27}$$

$$G_m = \frac{E_m}{2(1+\upsilon_m)}. \tag{28}$$

Morever, α and β in Eqs. (17) and (18) are given as follows

$$\alpha = \frac{(1+\upsilon_{out})}{3(1-\upsilon_{out})}, \tag{29}$$

$$\alpha = \frac{(1+\upsilon_{out})}{3(1-\upsilon_{out})} \quad , \tag{30}$$

$$\upsilon_{out} = \frac{3K_{out} - 2G_{out}}{6K_{out} + 2G_{out}}. \tag{31}$$

Therefore, the effective Young's modulus E and Poisson's ratio v of the composite material are given by

$$E = \frac{9KG}{3K+G} \quad , \tag{32}$$

$$\upsilon = \frac{3K-2G}{6K+2G}. \tag{33}$$

4. Energy method

To derive the governing equations of the structure by employing energy method and using Hamilton's principle, the work done by external forces is equated to the strain energy and kinetic energy stored in the structure. The potential strain energy stored in the structure is given as follows

$$U = \int_{V_c} \left(\sigma_{xx}^c \varepsilon_{xx} + \tau_{xz}^c \varepsilon_{xz}\right) dA_c dx + \int_{V_f} \left(\sigma_{xx}^f \varepsilon_{xx} + \tau_{xz}^f \varepsilon_{xz}\right) dA_f dx, \tag{34}$$

where A_c and A_f are the cross section area of the concrete column and NFRP layer, respectively. By substituting Eqs. (3) and (4) into Eq. (34) we have

$$\begin{aligned} U = {} & \frac{1}{2}\int_0^L \left[\int_{A_c} \left[\sigma_{xx}^c \left\{ \frac{\partial u}{\partial x} - z\frac{\partial^2 w}{\partial x^2} + \frac{1}{2}\left(\frac{\partial w}{\partial x}\right)^2 + f\frac{\partial \psi}{\partial x} \right\} \right.\right. \\ & \left.\left. + \tau_{xz}^c \left\{ \cos\left(\frac{\pi z}{h}\right)\psi \right\} \right] dA_c dx \\ & + \frac{1}{2}\int_0^L \left[\int_{A_f} \left[\sigma_{xx}^f \left\{ \frac{\partial u}{\partial x} - z\frac{\partial^2 w}{\partial x^2} + \frac{1}{2}\left(\frac{\partial w}{\partial x}\right)^2 + f\frac{\partial \psi}{\partial x} \right\} \right.\right. \\ & \left.\left. + \tau_{xz}^f \left\{ \cos\left(\frac{\pi z}{h}\right)\psi \right\} \right] dA_f dx. \end{aligned} \tag{35}$$

By defining the in-plane stress resultants as follows

$$N_x = \int_{A_c} \sigma_{xx}^c dA_c + \int_{A_f} \sigma_{xx}^f dA_f, \tag{36}$$

$$M_x = \int_{A_c} \sigma_{xx}^c z dA_c + \int_{A_f} \sigma_{xx}^f z dA_f, \tag{37}$$

$$F_x = \int_{A_c} \sigma_{xx}^c f dA_c + \int_{A_f} \sigma_{xx}^f f\, dA_f, \tag{38}$$

$$Q_x = \int_{A_c} \tau_{xz}^c \frac{\partial f}{\partial z} dA_c + \int_{A_f} \tau_{xz}^f \frac{\partial f}{\partial z} dA_f, \tag{39}$$

Eq. (35) can be rewritten as below

$$\begin{aligned} U = {} & \frac{1}{2}\int_0^L \left[\int \left[N_x \left(\left(\frac{\partial U}{\partial x}\right) + \left(\frac{1}{2}\left(\frac{\partial W}{\partial x}\right)^2\right) \right) - M_x \left(\frac{\partial^2 W}{\partial x^2}\right) \right.\right. \\ & \left.\left. + F_x \left(\frac{\partial \psi}{\partial x}\right) + Q_x(\psi) \right] dx, \end{aligned} \tag{40}$$

By substituting Eqs. (5)-(8) into Eqs. (36)-(39), the stress resultants of the column take the following form

$$N_x = A_{11}\left(\frac{\partial U}{\partial x} + \frac{1}{2}\left(\frac{\partial W}{\partial x}\right)^2\right) - B_{11}\left(\frac{\partial^2 W}{\partial x^2}\right) + E_{11}\frac{\partial \psi}{\partial x}, \tag{41}$$

$$M_x = B_{11}\left(\frac{\partial U}{\partial x} + \frac{1}{2}\left(\frac{\partial W}{\partial x}\right)^2\right) - D_{11}\left(\frac{\partial^2 W}{\partial x^2}\right) + F_{11}\frac{\partial \psi}{\partial x}, \tag{42}$$

$$F_x = E_{11}\left(\frac{\partial U}{\partial x} + \frac{1}{2}\left(\frac{\partial W}{\partial x}\right)^2\right) - F_{11}\left(\frac{\partial^2 W}{\partial x^2}\right) + H_{11}\frac{\partial \psi}{\partial x}, \tag{43}$$

$$Q_x = L_{44}\psi, \tag{44}$$

in which

$$A_{11} = \int_{A_c} C_{11} dA_c + \int_{A_f} Q_{11} dA_f, \tag{45}$$

$$B_{11} = \int_{A_c} C_{11} z dA_c + \int_{A_f} Q_{11} z dA_f, \tag{46}$$

$$D_{11} = \int_{A_c} C_{11} z^2 dA_c + \int_{A_f} Q_{11} z^2 dA_f, \tag{47}$$

$$E_{11} = \int_{A_c} C_{11} f dA_c + \int_{A_f} Q_{11} f dA_f, \tag{48}$$

$$F_{11} = \int_{A_c} C_{11} z f dA_c + \int_{A_f} Q_{11} z f dA_f, \tag{49}$$

$$H_{11} = \int_{A_c} C_{11} f^2 dA_c + \int_{A_f} Q_{11} f^2 dA_f, \tag{50}$$

$$L_{44} = \int_{A_c} C_{11} \frac{\partial f}{\partial z} dA_c + \int_{A_f} Q_{11} \frac{\partial f}{\partial z} dA_f. \tag{51}$$

The kinetic energy of the structure are defined as below

$$K = \frac{\rho}{2}\int \left(\dot{u}_1^2 + \dot{u}_2^2 + \dot{u}_3^2\right) dV \tag{52}$$

By substituting Eq. (1) into Eq. (52) we have

$$K = \frac{\rho}{2}\int \left(\left(\frac{\partial u}{\partial t} - z\frac{\partial^2 w}{\partial x\, \partial t} + f\left(\frac{\partial \psi}{\partial t}\right)\right)^2 + \left(\frac{\partial w}{\partial t}\right)^2 \right) dV. \tag{53}$$

By defining the inertia moment terms as

$$\begin{Bmatrix} I_0 \\ I_1 \\ I_2 \\ I_3 \\ I_4 \\ I_5 \end{Bmatrix} = \int_{A_c} \begin{bmatrix} \rho_c \\ \rho_c z \\ \rho_c z^2 \\ \rho_c f \\ \rho_c z f \\ \rho_c f^2 \end{bmatrix} dA_c + \int_{A_f} \begin{bmatrix} \rho_f \\ \rho_f z \\ \rho_f z^2 \\ \rho_f f \\ \rho_f z f \\ \rho_f f^2 \end{bmatrix} dA_f , \tag{54}$$

where ρ_c and ρ_f are concrete and NFRP densities, respectively. Eq. (53) can be rewritten as below

$$K = 0.5\int \left[I_0 \left(\left(\frac{\partial u}{\partial t}\right)^2 + \left(\frac{\partial w}{\partial t}\right)^2 \right) - 2I_1 \left(\frac{\partial u}{\partial t}\frac{\partial^2 w}{\partial x \partial t} \right) + I_2 \left(\frac{\partial^2 w}{\partial x \partial t} \right)^2 + I_3 \frac{\partial u}{\partial t}\frac{\partial \psi}{\partial t} - I_4 \frac{\partial^2 w}{\partial x \partial t}\frac{\partial \psi}{\partial t} + I_5 \left(\frac{\partial \psi}{\partial t} \right)^2 \right] dx . \tag{55}$$

The external work due the earthquake can be calculated as follows

$$W = \int_{F_{Seismic}} (ma(t))w dx , \tag{56}$$

where m and $a(t)$ are the mass and acceleration of the earth, respectively. To extract the governing equations of motion, Hamilton's principle is expressed as follows

$$\int_0^t (\delta U - \delta K - \delta W) dt = 0, \tag{57}$$

where δ denotes the variational operator. By considering Eqs. (40), (55) and (56), the motion equations of the structure are obtained as follows

δU :

$$\frac{\partial N_x}{\partial x} = I_0 \frac{\partial^2 u}{\partial t^2} + (I_3 - I_1)\frac{\partial^3 w}{\partial x \partial t^2} - I_3 \frac{\partial^2 \psi}{\partial t^2}, \tag{58}$$

δW :

$$\begin{aligned} &\frac{\partial^2 M_x}{\partial x^2} - \frac{\partial^2 F_x}{\partial x^2} + \frac{\partial Q_x}{\partial x} + F_{Seismic} \\ &= I_0 \frac{\partial^2 w}{\partial t^2} + (I_1 - I_3)\frac{\partial^3 u}{\partial x \partial t^2} + (2I_4 - I_2 - I_5)\frac{\partial^4 w}{\partial x^2 \partial t^2} \\ &+ (I_5 - I_4)\frac{\partial^3 \psi}{\partial x \partial t^2}, \end{aligned} \tag{59}$$

$\delta\varphi$:

$$Q_x - \frac{\partial F_x}{\partial x} = I_5 \frac{\partial^2 \psi}{\partial t^2} - I_3 \frac{\partial^2 u}{\partial t^2} + (I_4 - I_5)\frac{\partial^3 w}{\partial x \partial t^2}, \tag{60}$$

Also, the boundary conditions of the structure are considered as below

• Clamped-clamped supported

$$\begin{aligned} &w = u = \psi = \frac{\partial w}{\partial x} = 0, && @ \quad x = 0 \\ &w = u = \psi = \frac{\partial w}{\partial x} = 0. && @ \quad x = L \end{aligned} \tag{61}$$

• Clamped-Simply supported

$$\begin{aligned} &w = u = \psi = \frac{\partial w}{\partial x} = 0, && @ \quad x = 0 \\ &w = u = \psi = M_x = 0. && @ \quad x = L \end{aligned} \tag{62}$$

• Simply-Simply supported

$$\begin{aligned} &w = u = \psi = M_x = 0, && @ \quad x = 0 \\ &w = u = \psi = M_x = 0. && @ \quad x = L \end{aligned} \tag{63}$$

5. Solution procedure

In this study, HDQM is applied to examine the dynamic behavior of the structure. In this numerical method, the governing differential equations of the structure turn into a set of first order algebraic equations by applying the weighting coefficients. According to HDQ method, a derivative of a function at a given discrete point will be approximated as a weighted linear sum of the function values at all discrete points chosen in the solution domain. The one-dimensional derivative of the function can be expressed as follows (Kolahchi *et al.* 2016a , b)

$$\frac{d^n f(x_i)}{dx^n} = \sum_{j=1}^{N} C_{ij}^{(n)} f(x_j) \qquad n = 1,..., N-1. \tag{64}$$

Where $f(x)$ is the mentioned function, N denotes number of grid points, x_i is a sample point of the function domain, f_i is the value of the function at ith sample point and C_{ij} indicates the weighting coefficients. So, choosing the grid points and weighting coefficients is an important factor in the accuracy of the results. The grid points are considered by Chebyshev polynomials as follows

$$X_i = \frac{L}{2}\left[1 - \cos\left(\frac{i-1}{N_x - 1} \right)\pi \right] \quad i = 1,..., N_x \tag{65}$$

Based on Chebyshev polynomials, the grid points are closer together near the borders and in distant parts of the borders they aw y from each other. The weighting coefficients may be calculated by the following simple algebraic relations

$$A_{ij}^{(1)} = \begin{cases} \dfrac{(\pi/2)M(x_i)}{M(x_j)\sin[(x_i - x_j)/2]\pi} & for \quad i \neq j, \quad i, j = 1,2,..., N_x, \\ -\sum\limits_{\substack{j=1 \\ i \neq j}}^{N_x} A_{ij}^{(1)} & for \quad i = j, \quad i, j = 1,2,..., N_x \end{cases} \tag{66}$$

in which

$$M(x_i) = \prod_{\substack{j=1 \\ j \neq i}}^{N_x} \sin\left(\frac{(x_i - x_j)\pi}{2} \right) \tag{67}$$

Also, the higher-order derivatives are considered as

$$A_{ij}^{(n)} = n\left(A_{ii}^{(n-1)} A_{ij}^{(1)} - \pi ctg\left(\frac{x_i - x_j}{2} \right)\pi \right) \tag{68}$$

By distributing the grid points in the domain based on Eq. (65) and by substituting Eq. (64) into the governing equations, we have

$$\left(\left[\underbrace{K_L + K_{NL}}_{K} \right] \begin{Bmatrix} \{d_b\} \\ \{d_d\} \end{Bmatrix} + [M] \begin{Bmatrix} \{\ddot{d}_b\} \\ \{\ddot{d}_d\} \end{Bmatrix} \right) = \begin{Bmatrix} \{0\} \\ -Ma(t) \end{Bmatrix}, \tag{69}$$

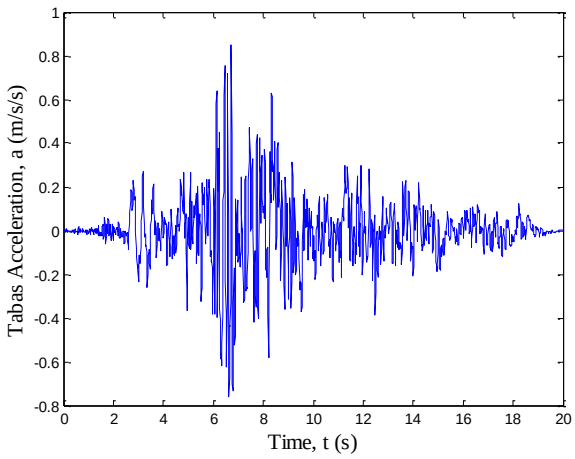

Fig. 2 Acceleration history of Kobe earthquake

in which $[K_L]$, $[K_{NL}]$ and $[M]$ indicate linear part of the stiffness matrix, nonlinear part of the stiffness matrix and the mass matrix, respectively. Also, $\{d_b\}$ and $\{d_d\}$ denote boundary and domain points, respectively. To obtain the time response of the structure subjected to the earthquake loads Newmark method (Simsek 2010) is applied in the time domain. Based on this method, Eq. (69) is considered in the general form as below

$$K^*(d_{i+1}) = Q_{i+1}, \tag{70}$$

where subscript i+1 denotes the time $t=t_{i+1}$, $K^*(d_{i+1})$ and Q_{i+1} are the effective stiffness matrix and the effective load vector which are given as

$$K^*(d_{i+1}) = K_L + K_{NL}(d_{i+1}) + \alpha_0 M + \alpha_1 C, \tag{71}$$

$$Q^*_{i+1} = Q_{i+1} + M\left(\alpha_0 d_i + \alpha_2 \dot{d}_i + \alpha_3 \ddot{d}_i\right) + C\left(\alpha_1 d_i + \alpha_4 \dot{d}_i + \alpha_5 \ddot{d}_i\right), \tag{72}$$

where (Simsek 2010)

$$\alpha_0 = \frac{1}{\chi \Delta t^2}, \quad \alpha_1 = \frac{\gamma}{\chi \Delta t}, \quad \alpha_2 = \frac{1}{\chi \Delta t}, \quad \alpha_3 = \frac{1}{2\chi} - 1, \quad \alpha_4 = \frac{\gamma}{\chi} - 1,$$
$$\alpha_5 = \frac{\Delta t}{2}\left(\frac{\gamma}{\chi} - 2\right), \quad , \alpha_6 = \Delta t(1-\gamma), \quad \alpha_7 = \Delta t \gamma, \tag{73}$$

where γ=0.5 and χ=0.25. By applying the iteration method, Eq. (70) is solved at any time step and modified velocity and acceleration vectors are computed as follows

$$\ddot{d}_{i+1} = \alpha_0 (d_{i+1} - d_i) - \alpha_2 \dot{d}_i - \alpha_3 \ddot{d}_i, \tag{74}$$

$$\dot{d}_{i+1} = \dot{d}_i + \alpha_6 \ddot{d}_i + \alpha_7 \ddot{d}_{i+1}, \tag{75}$$

Then for the next time step, the modified velocity and acceleration vectors in Eqs. (64) and (75) are applied and all the mentioned procedures are repeated.

6. Numerical results

In this section, the effect of various parameters on the dynamic response of the NFRP strengthened concrete column under seismic load is examined. The outer radius

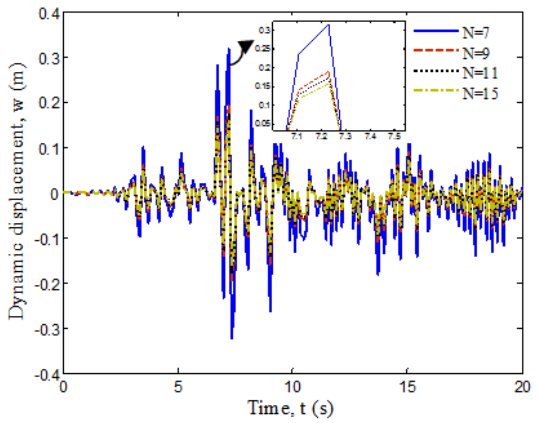

Fig. 3 Convergence and accuracy of HDQM

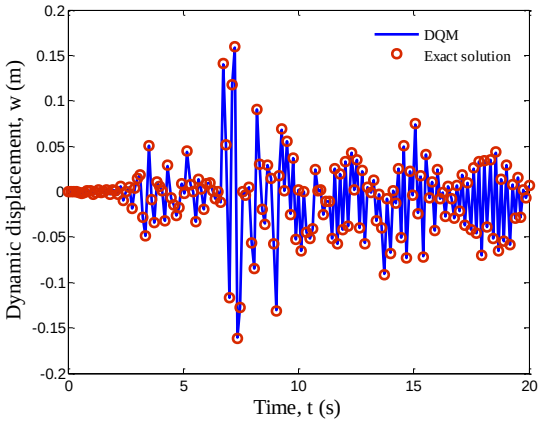

Fig. 4 Comparison of analytical and numerical results

and the inner radius of the concrete column are R_0=205 mm and R_i=56 mm, respectively and the length of the column is L=3 *m*. The elastic moduli of concrete, epoxy resin and carbon nanofiber are E_c=20 *Gpa*, E_f=25 *Gpa* and E_r=1 *TPa*, respectively. In this study, the influences of NFRP layer, carbon nanofiber volume fraction, geometric parameters and boundary conditions on the dynamic displacement of the structure are investigated. The earthquake acceleration is considered based on Tabas earthquake that the distribution of acceleration in 30 seconds is shown in Fig. 2.

6.1 Convergence of HDQM

Fig. 3 shows the convergence of HDQM in evaluating the maximum deflection of the structure versus time. As it can be seen, with increasing the number of grid points N, the maximum deflection of the structure decreases. It can be found that by increasing the number of grid points, the decay ratio of the dynamic deflection decreases as far as at N=15 the dynamic deflection converges.

6.2 Validation of results

Given that no similar work has been done to validate the present study, so, it has been tried to examine the results without considering the nonlinear terms of the governing equations and by comparing the linear dynamic response of the structure which obtained by two various solution

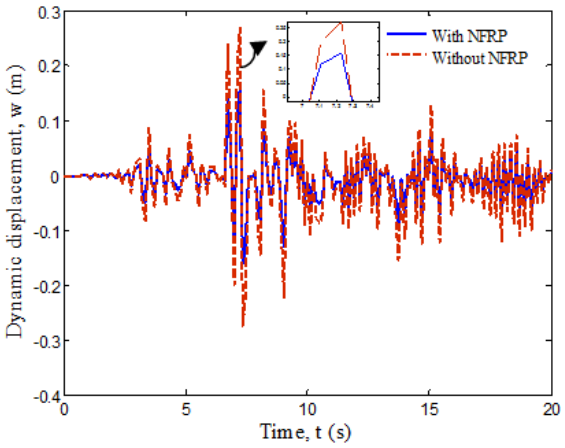

Fig. 5 The effect of NFRP layer on the dynamic deflection of the structure

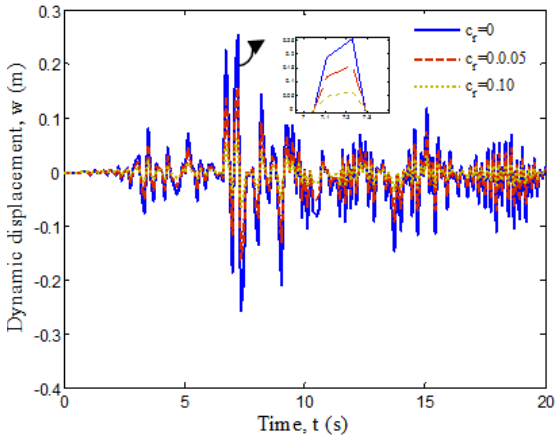

Fig. 6 The effect of nanofibers volume percent on the dynamic deflection of the structure

methods. The results of the analytical and numerical (HDQ) methods are depicted in Fig. 4. As it can be observed, the results of numerical and analytical methods are identical and therefore, the obtained results are accurate and acceptable.

6.3 Effects of different parameters

Fig. 5 illustrate the effect of NFRP layer on the dynamic deflection versus time and various thicknesses of the NFRP layer. As it can be observed, the structure without NFRP layer has a greater dynamic deflection with respect to the concrete column covered with a NFRP layer. The reason is that the NFRP layer increases the stiffness of the structure.

As mentioned in the previous sections, the NFRP is reinforced by carbon nanofibers instead of macro fibers. In this section, the effect of nanofibers volume percent on the dynamic response of the structure is studied. Fig.6 shows the dynamic deflection of the structure versus time for different values of nanofibers volume fraction. It can be seen that with increasing the nanofiber volume fraction, the displacement is decreased. So it can be concluded that with increasing the volume fraction of nanofibers, the dynamic deflection of the system decreases and it is because of the increasing of the stiffness of the structure.

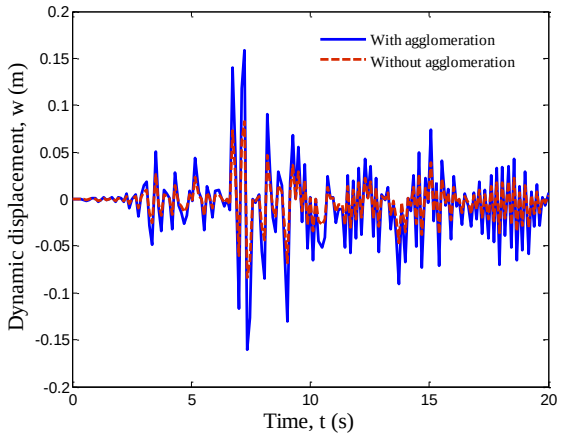

Fig. 7 The effect of nanofibers agglomeration on the dynamic deflection of the structure

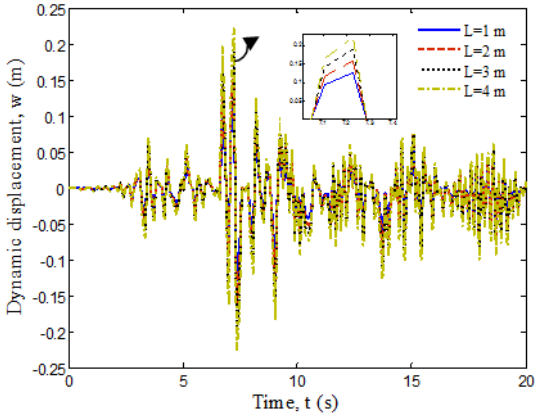

Fig. 8 The effect of column length on the dynamic deflection of the structure

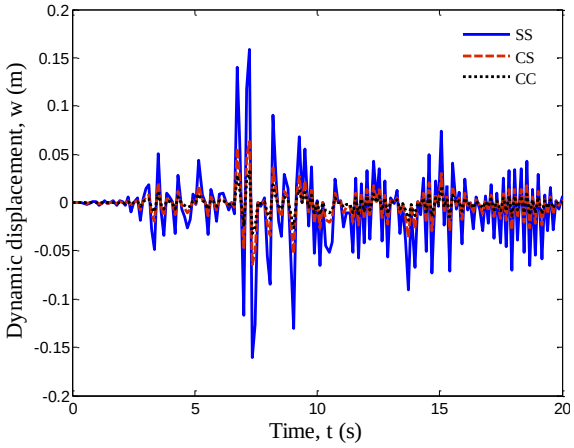

Fig. 9 The effect of boundary conditions on the dynamic deflection of the structure

The agglomeration effect of nanofibers on the dynamic deflection of the structure versus time is illustrated in Fig. 7. As it can be observed, by considering the agglomeration effect, the stiffness of the structure reduces while the dynamic displacement increases. Since during the process of nanocomposite manufacturing, the uniform distribution for nanofibersin the matrix is impossible, so the results of this figure can be very remarkable.

Fig. 8 presents the effect of the column length on the dynamic deflection of the structure versus time. It can be found that with increasing the length, the displacement of the structure increases. It is because of the reduction of the stiffness of the system when the column becomes longer.

Fig. 9 illustrate the effect of various boundary conditions on the dynamic response versus time. Four boundary conditions including clamped-clamped, clamped-simply, simply-simply and free-simply supported are considered. The minimum dynamic deflections of the structure are related to clamped-clamped, clamped-simply supported and simply-simply supported boundary conditions.

7. Conclusions

Seismic response of concrete columns covered by NFRP layer was studied in this paper. The SSDT was used for obtaining the motion equations. Mori-Tanaka model was utilized for considering agglomeration effect of nanofibers. Based on HDQM and Newmrk method, the dynamic deflection of the structure was calculated. The effects of different parameters such as NFRP layer, geometrical parameters of column, volume fraction and agglomeration of nanofibers and boundary conditions on the dynamic response of the structure were shown. The structure without NFRP layer has a greater dynamic deflection with respect to the concrete column covered with a NFRP layer. It can be seen that with increasing the nanofiber volume fraction, the displacement was decreased. Considering the agglomeration effect, the stiffness of the structure reduces while the dynamic displacement increases. It can be found that with increasing the length, the displacement of the structure increases. In addition, the minimum dynamic deflections of the structure were related to clamped-clamped boundary condition with respect to clamped-simply supported and simply-simply supported boundary conditions.

References

Arbabi, A., Kolahchi, R. and Rabani Bidgoli, M. (2017), "Concrete columns reinforced with Zinc Oxide nanoparticles subjected to electric field: Buckling analysis", *Wind Struct.*, **24**(5), 431-446.

Berradia, M. and Kassoul, A. (2017), "Combined effect of CFRP-TSR confinement on circular reinforced concrete columns", *Comput. Concrete*, **19**(1), 41-49.

El-Helou, R.G. and Aboutaha, R.S. (2015), "Analysis of rectangular hybrid steel-GFRP reinforced concrete beam columns", *Comput. Concrete*, **16**: 245-260.

Heidarzadeh, A., Kolahchi, R. and Rabani Bidgoli, M. (2016), "Concrete pipes reinforced with AL2O3 nanoparticles considering agglomeration: Magneto-thermo-mechanical stress analysis", *J. Civil Eng.*, 0130-2.

Jafarian Arani, A. and Kolahchi, R. (2016), "Buckling analysis of embedded concrete columns armed with carbon nanotubes", *Comput. Concrete*, **17**(5), 567-578.

Kang, J.W. and Lee, J. (2016), "A new damage index for seismic fragility analysis of reinforced concrete columns", *Struct. Eng. Mech.*, **60**(5), 875-890.

Kolahchi, R., Rabani Bidgoli, M., Beygipoor, G. and Fakhar, M.H. (2016a), "A nonlocal nonlinear analysis for buckling in embedded FG-SWCNT-reinforced microplates subjected to magnetic field", *J. Mech. Sci. Technol.*, **5**, 2342-2355.

Kolahchi, R., Safari, M. and Esmailpour, M. (2016b), "Dynamic stability analysis of temperature-dependent functionally graded CNT-reinforced visco-plates resting on orthotropic elastomeric medium", *Compos. Struct.*, **150**, 255-265.

Kumar, V. and Patel, P.V. (2016), "Strengthening of axially loaded concrete columns using stainless steel wire mesh (SSWM)-numerical investigations", *Struct. Eng. Mech.*, **60**(6), 979-999.

Lee, D.H., Cheon, N.R., Kim, M., Lee, J., Oh, J.Y. and Kim, K.S. (2017), "Simplified P-M interaction curve model for reinforced concrete columns exposed to standard fire", *Comput. Concrete*, **19**(5), 545-553.

Mori, T. and Tanaka, K. (1973), "Average stress in matrix and average elastic energy of materials with misfitting inclusions", *Acta Metall. Mater.*, **21**(5), 571-574.

Nematzadeh, M. and Haghinejad, A. (2017), "Analysis of actively-confined concrete columns using prestressed steel tubes", *Comput. Concrete*, **19**(5), 477-488.

Safari Bilouei, B., Kolahchi, R. and Rabani Bidgol, M. (2016), "Buckling of concrete columns retrofitted with nano-fiber reinforced polymer (NFRP)", *Comput. Concrete*, **18**(5), 1053-1063.

Shu, C. and Xue, H. (1997), "Explicit computations of weighting coefficients in the harmonic differential quadrature", *J. Sound Vibr.*, **204**(3), 549-555.

Simsek, M. (2010), "Non-linear vibration analysis of a functionally graded Timoshenko beam under action of a moving harmonic load", *Compos. Struct.*, **92**(10), 2532-2546.

Thai, H.T. and Vo, T.P. (2012), "A nonlocal sinusoidal shear deformation beam theory with application to bending, buckling, and vibration of nanobeams", *J. Eng. Sci.*, **54**, 58-66.

Truong, G.T., Kim, J.C. and Choi, K.K. (2017), "Seismic performance of reinforced concrete columns retrofitted by various methods", *Eng. Struct.*, **134**, 217-235.

Yan, C.W., Jia, J. and Zhang, J. (2010), "Seismic behavior of steel reinforced ultra high strength concrete column and reinforced concrete beam connection", *Trans. Tianjin Univ.*, **16**(4), 309-316.

Zamanian, M., Kolahchi, R. and Rabani Bidgoli, M. (2016), "Agglomeration effects on the buckling behaviour of embedded concrete columns reinforced with SiO2 nano-particles", *Wind Struct.*, **24**(1), 43-57.

Zong-Cai, D., Daud, J.R. and Hui, L. (2014), "Seismic behavior of short concrete columns with prestressing steel wires", *Adv. Mater. Sci. Eng.*, **21**, 180193.

CC